J|A|C|S ARTICLES

Published on Web 02/01/2010

Role of Ceria in Oxidative Dehydrogenation on Supported Vanadia Catalysts

Maria Veronica Ganduglia-Pirovano,*[,†,‡] Cristina Popa,[†] Joachim Sauer,[†] Heather Abbott,[§] Alexander Uhl,[§] Martin Baron,[§] Dario Stacchiola,[§] Oleksandr Bondarchuk,[§] Shamil Shaikhutdinov,*[,§] and Hans-Joachim Freund[§]

Institute of Chemistry, Humboldt Universität zu Berlin, Unter den Linden 6, 10099 Berlin, Germany, and Chemical Physics Department, Fritz Haber Institut der Max Planck Gesellschaft, Faradayweg 4−6, 14195 Berlin, Germany

Received December 15, 2009; E-mail: vgp@chemie.hu-berlin.de; shaikhutdinov@fhi-berlin.mpg.de

Abstract: The effect of the suppport on oxidative dehydrogenation activity for vanadia/ceria systems is examined for the oxidation of methanol to formaldehyde by use of well-defined $VO_x/CeO_2(111)$ model catalysts. Temperature-programmed desorption at low vanadia loadings revealed reactivity at much lower temperature (370 K) as compared to pure ceria and vanadia on inert supports such as silica. Density functional theory is applied and the energies of hydrogenation and oxygen vacancy formation also predict an enhanced reactivity of the vanadia/ceria system. At the origin of this support effect is the ability of ceria to stabilize reduced states by accommodating electrons in localized f-states.

1. Introduction

Vanadium oxide is the major active component of catalysts for selective oxidation reactions.[1−4] The activity of supported vanadia is strongly affected by the specific oxide used as a support.[2,3,5,6] In oxidative dehydrogenation (ODH) reactions, vanadia supported on ceria shows a remarkably high activity as compared to silica- and alumina-supported catalysts.[2,6,7] Although cerium oxide is known for its ability to store, release, and transport oxygen ions,[8] the origin of the promoting effects of ceria in oxidation reactions has yet to be elucidated.

In this work, we focus on understanding the support effect on the ODH activity for vanadia/ceria catalysts. We employ a well-defined $VO_x/CeO_2(111)$ model system, for which the atomic surface structure has been determined,[9] and we study the selective oxidation of methanol to formaldehyde as a prototype ODH reaction, because alkane oxidation typically requires high pressures and temperatures. Nevertheless, in both alcohol and alkane ODH on metal oxides the rate-limiting step is a reduction−oxidation (redox) process, which involves C−H bond cleavage.[10−12] For vanadium oxide species supported on silica, previous calculations based on density functional theory (DFT) have indeed shown that the rate-determining step is H abstraction from a C−H bond,[13,14] as found in many other cases including homogeneous and enzymatic catalysis.[15] Before this can happen, the reactant molecule needs to bind onto the surface. This initial binding is of van der Waals type in the case of propane[14] but an acid−base type chemisorption in the case of methanol, leading to a hydroxy (by transfer of the methanol proton) and a methoxy group on the catalyst surface.[13,16]

Our temperature-programmed reaction experiments reveal that methanol oxidation to formaldehyde on the VO_x/CeO_2 model catalyst may occur at much lower temperature than previously reported for supported vanadia catalysts.[17−22] This observation is rationalized by density functional theory (DFT) calculations

[†] Humboldt Universität zu Berlin.

[‡] Present address: Institute of Catalysis and Petrochemistry, CSIC, C/Marie Curie 2, 28049 Madrid, Spain.

[§] Fritz Haber Institut der Max Planck Gesellschaft.

(1) Weckhuysen, B. M.; Keller, D. E. *Catal. Today* **2003**, *78*, 25–46.
(2) Wachs, I. E. *Catal. Today* **2005**, *100*, 79–94.
(3) Bañares, M. A. *Catal. Today* **1999**, *51* (2), 319–348.
(4) Blasco, T.; Nieto, J. M. L. *Appl. Catal., A* **1997**, *157*, 117–142.
(5) Khodakov, A.; Olthof, B.; Bell, A. T.; Iglesia, E. *J. Catal.* **1999**, *181*, 205–216.
(6) Dinse, A.; Frank, B.; Hess, C.; Habel, D.; Schomacker, R. *J. Mol. Catal. A* **2008**, *289*, 28–37.
(7) Daniell, W.; Ponchel, A.; Kuba, S.; Anderle, F.; Weingand, T.; Gregory, D. H.; Knozinger, H. *Top. Catal.* **2002**, *20* (1−4), 65–74.
(8) Trovarelli, A. *Catalysis by Ceria and Related Materials*; Catalytic Science Series; Imperial College Press: London, 2002; Vol. 2.
(9) Baron, M.; Abbott, H. L.; Bondarchuk, O.; Stacchiola, D.; Uhl, A.; Shaikhutdinov, S.; Freund, H.-J.; Popa, C.; Ganduglia-Pirovano, M. V.; Sauer, J. *Angew. Chem., Int. Ed.* **2009**, *48*, 8006–8009.
(10) Argyle, M. D.; Chen, K. D.; Bell, A. T.; Iglesia, E. *J. Phys. Chem. B* **2002**, *106* (21), 5421–5427.
(11) Kilos, B.; Bell, A. T.; Iglesia, E. *J. Phys. Chem. C* **2009**, *113* (7), 2830–2836.
(12) Chen, K. D.; Iglesia, E.; Bell, A. T. *J. Phys. Chem. B* **2001**, *105* (3), 646–653.
(13) Döbler, J.; Pritzsche, M.; Sauer, J. *J. Am. Chem. Soc.* **2005**, *127*, 10861–10868.
(14) Rozanska, X.; Fortrie, R.; Sauer, J. *J. Phys. Chem. C* **2007**, *111*, 6041–6050.
(15) Limberg, C. *Angew. Chem., Int. Ed.* **2003**, *42*, 5932–5954.
(16) Romanyshyn, Y.; Guimond, S.; Kuhlenbeck, H.; Kaya, S.; Blum, R. P.; Niehus, H.; Shaikhutdinov, S.; Simic-Milosevic, V.; Nilius, N.; Freund, H.-J.; Ganduglia-Pirovano, M. V.; Fortrie, R.; Döbler, J.; Sauer, J. *Top. Catal.* **2008**, *50*, 106–115.
(17) Wong, G. S.; Concepcion, M. R.; Vohs, J. M. *Surf. Sci.* **2003**, *526* (3), 211–218.
(18) Feng, T.; Vohs, J. M. *J. Catal.* **2004**, *221* (2), 619–629.
(19) Feng, T.; Vohs, J. M. *J. Phys. Chem. B* **2005**, *109*, 2120–2127.
(20) Wong, G. S.; Concepcion, M. R.; Vohs, J. M. *J. Phys. Chem. B* **2002**, *106* (25), 6451–6455.
(21) Wang, Q. G.; Madix, R. J. *Surf. Sci.* **2002**, *496* (1−2), 51–63.
(22) Burcham, L. J.; Wachs, I. E. *Catal. Today* **1999**, *49*, 467.

for monomeric VO_2 adspecies on the $CeO_2(111)$ surface with VO_4 coordination.

Relying on energies for hydrogenation and oxygen vacancy formation as descriptors for ODH reactions,[23,24] we show that upon H transfer from methanol (as upon other reduction reactions such as O defect formation), monomeric vanadia species remain in the +5 oxidation state, whereas Ce ions are reduced from $Ce(f^0)^{4+}$ to $Ce(f^1)^{3+}$. We conclude that reduction of the ceria support is the key factor determining the superior activity of ceria supported vanadia catalysts.

2. Experiments

2.1. Details. The experiments were carried out in an ultrahigh vacuum chamber (base pressure $\sim 5 \times 10^{-10}$ mbar) equipped with low energy electron diffraction (LEED), Auger electron spectroscopy, infrared reflection absorption spectroscopy (IRAS), and a quadrupole mass spectrometer (QMS) for temperature-programmed desorption (TPD) measurements. The well-ordered, fully oxidized $CeO_2(111)$ thin films of ~3 nm average thickness were grown on a Ru(0001) substrate as described previously.[25−27] Vanadium (Goodfellow, 99.8%) was deposited via physical vapor deposition in 10^{-6} mbar of O_2 onto the ceria film at <150 K and subsequently annealed to 300 K in the same oxygen ambient. The vanadium deposition rate was calibrated using a quartz microbalance, while scanning tunneling microscopy (STM) was used in the previous IRAS-STM study.[9] This may cause deviations in the absolute values for vanadia coverage, but it does not affect the general trend observed by IRAS in both experimental setups.

Approximately 5 L (1 L = 10^{-6} Torr s) of methanol (Merck, 99.8%, additionally purified by repeated freeze/pump/thaw cycles) was deposited onto vanadia/ceria samples at 300 K by use of a directional gas doser. QMS signal intensities were corrected for the cracking pattern of methanol in our spectrometer.

2.2. Results. At low vanadia loadings, a combination of STM, IRAS, and X-ray photoelectron spectroscopy (XPS) showed the formation of isolated monomeric species as well as of two-dimensional clusters that wet the ceria support as previously assumed for the real "monolayer"-type catalysts. The vanadia species exhibit V in +5 oxidation state and expose vanadyl (V═O) groups. At high vanadia coverage, three-dimensional vanadia nanoparticles are formed that resemble V═O-terminated V_2O_3 particles as monitored by XPS.

TPD spectra of the major desorption products after exposure of the $VO_x/CeO_2(111)$ model catalysts to methanol at room temperature are presented in Figure 1. The pristine $CeO_2(111)$ film shows a formaldehyde desorption signal at 565 K (γ peak; see also refs 18 and 28). Upon vanadia deposition, the γ peak shifts to 590 K. Similar observations have been reported for reduced ceria films.[28] Additionally, two new peaks appear at lower temperatures, denoted as α at 370 K and β at 475 K. At high vanadia coverage, the α and γ peaks disappear and the β peak shifts to 505 K. Desorption features similar to the β peak have been observed on silica-supported vanadia[16] and other model systems such as single-crystal vanadia surfaces[16,29] and ceria-supported vanadia films,[20] all of which have desorption peak intensities between 450 and 590 K. Thus, the β peak can be assigned straightforwardly to methanol ODH on vanadia nanoparticles and large oligomers imaged by STM at these coverages (see the inset in the bottom panel of Figure 1).

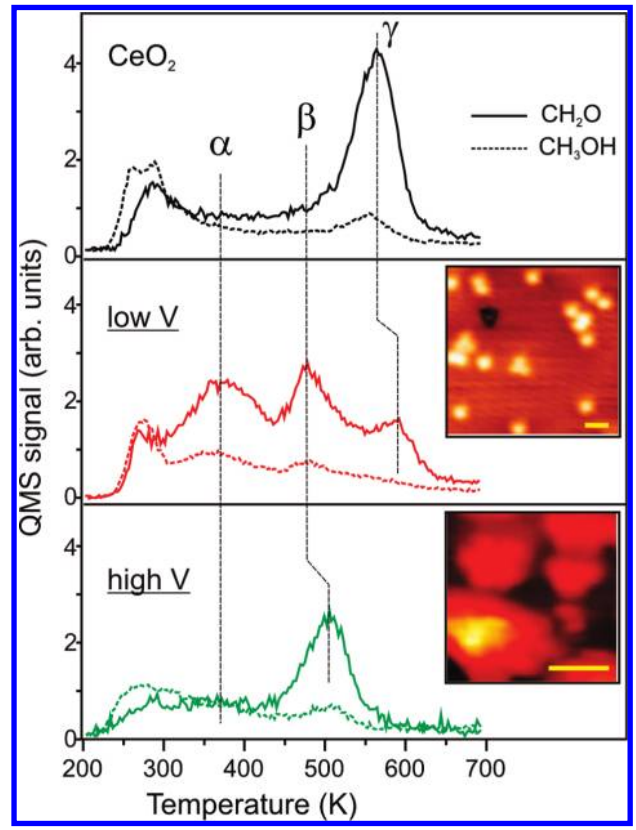

Figure 1. TPD spectra for ~5 L of CH_3OH adsorbed at 300 K on $CeO_2(111)$ and VO_x/CeO_2 (111) surfaces at low (<2 V at/nm^2) and high (~4 V at/nm^2) vanadia loadings. Solid lines indicate the raw signal for CH_3OH (31 amu), whereas dashed lines indicate CH_2O (29 amu, corrected for the methanol cracking pattern). Signal intensity below 300 K is assigned to the tail of CH_3OH monolayer desorption. The insets show typical STM images of vanadia species at the respective coverage. The scale bar corresponds to 1 nm.

In contrast, the α peak is observed at much lower temperature and at coverages where primarily monomeric vanadia species have been identified on these samples by IRAS following the structure−spectroscopy relationship established in ref 9 between the V═O stretching frequency and the nuclearity of vanadia species. The inset in the middle panel of Figure 1 shows a typical STM image of isolated monomeric species that dominate the surface, although dimers and trimers can be observed as well. By use of the Redhead formula[30] with a heating rate of 3 K/s and a frequency factor of 10^{13} s^{-1}, the desorption energies have been estimated as 1.0, 1.3, and 1.5−1.6 eV for the α, β, and γ peaks, respectively.

(23) Sauer, J. In *Computational Modeling for Homogeneous and Enzymatic Catalysis*; Morokuma, K., Musaev, D. G., Eds.; Wiley−VCH: Weinheim, Germany, 2008; pp 231−244.
(24) Sauer, J.; Döbler, J. *Dalton Trans.* **2004**, *19*, 3116–3121.
(25) Baron, M.; Bondarchuk, O.; Stacchiola, D.; Shaikhutdinov, S.; Freund, H.-J. *J. Phys. Chem. C* **2009**, *113*, 6042–6049.
(26) Lu, J. L.; Gao, H. J.; Shaikhutdinov, S.; Freund, H. J. *Surf. Sci.* **2006**, *600* (22), 5004–5010.
(27) Mullins, D. R.; Radulovic, P. V.; Overbury, S. H. *Surf. Sci.* **1999**, *429* (1−3), 186–198.
(28) Mullins, D. R.; Robbins, M. D.; Zhou, J. *Surf. Sci.* **2006**, *600* (7), 1547–1558.
(29) Göbke, D.; Romanyshyn, Y.; Guimond, S.; Sturm, J. M.; Kuhlenbeck, H.; Döbler, J.; Reinhardt, U.; Ganduglia-Pirovano, M. V.; Sauer, J.; Freund, H.-J. *Angew. Chem., Int. Ed.* **2009**, *48* (20), 3695–3698.
(30) Redhead, P. A. *Vacuum* **1963**, *12*, 203–211.

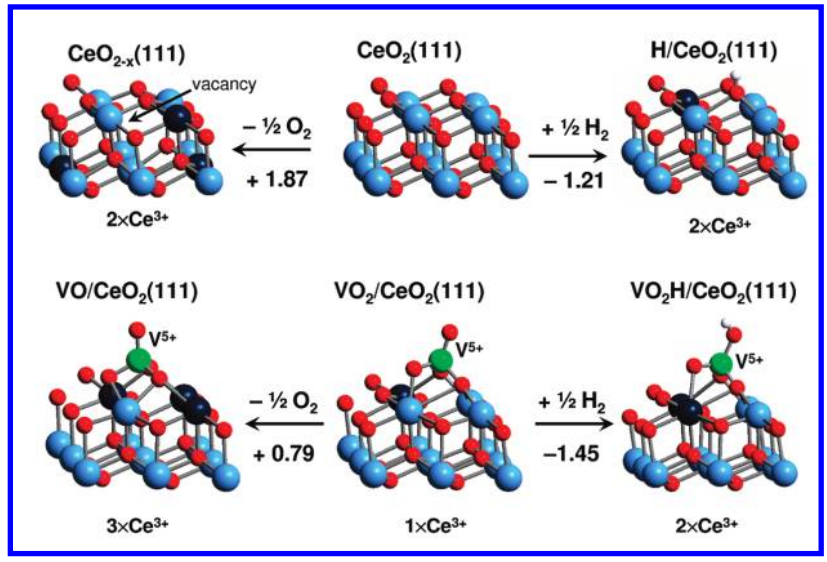

Figure 2. Top: Side views of the fully oxidized $CeO_2(111)$ surface (middle), the reduced $CeO_2(111)$ surface with a subsurface oxygen vacancy (left), and the hydrogenated $CeO_2(111)$ surface (right). Bottom: Side views of VO and VO_2 species on the defect-free $CeO_2(111)$ surface (left and middle) as well as of the hydrogenated $VO_2/CeO_2(111)$ surface (right). Large light and dark blue spheres represent Ce^{4+} and $Ce^{3+}(f^1)$ ions, respectively. V ions are represented as green spheres. Small red and white spheres represent O and H atoms, respectively. Reaction energies are given in electronvolts.

3. DFT Calculations

VO_n ($n = 1-4$) gas-phase species have been deposited on clean and defective (i.e., with one oxygen vacancy) $CeO_2(111)$ surfaces and the lowest energy structures have been determined. Differently from Shapovalov and Metiu,[31] who were the first to study these structures by DFT, we apply the DFT+U approach as implemented in the VASP package[32] to describe the on-site Coulomb interactions in the Ce 4f states. The latter approach was also used in studying methanol adsorption on the $CeO_2(111)$ surface.[33]

To identify the thermodynamically stable monomeric species for a given oxygen partial pressure at a given temperature, we have calculated the surface-related free energies of formation of these species[34,35]

$$\Delta\gamma_f = (1/A)(\Delta E_f - n\Delta\mu_O(p,T))$$

from the surface area A, the oxygen chemical potential relative to its value at 0 K, $\mu_{O_2}(T = 0\ \mathrm{K}) = E[O_2]$

$$\Delta\mu_O(p,T) = \frac{1}{2}\{\mu_{O_2}(T,p) - E[O_2]\}$$

and their energy of formation from the clean CeO_2 surface, solid vanadium, and molecular oxygen

$$\Delta E_f = (E[VO_n{\bullet}(CeO_2)_{12}] - E[(CeO_2)_{12}] - E[\{V\}_s] - \frac{n}{2}E[O_2])$$

neglecting vibrational contributions and the pV term of solid components.

3.1. Details. The spin-polarized calculations employed the PBE functional with a Hubbard U parameter of 4.5 eV for the Ce f-electrons, which was calculated self-consistently by Fabris et al.[36] This value is within the range 3.0−5.5 eV reported[37] to provide localization of the two electrons left upon oxygen removal from CeO_2. Test calculations with an additional Hubbard U parameter of 2.0 or 4.5 eV for the V d-states were performed, which led to the same localization in Ce f-states of the electrons resulting from reduction as the calculation without U for the V d-states. The changes in the calculated hydrogenation energies were on the order of 0.01 eV only.

The projector augmented wave method (PAW) was used at a plane-wave cutoff of 400 eV to decouple the core from valence electrons. The Ce (4f, 5s, 5p, 5d, 6s), O (2s, 2p), and V (3p, 3d, 4s) electrons were treated as valence states. The $CeO_2(111)$ surface was modeled by a supercell with nine atomic layers with calculated CeO_2 bulk equilibrium lattice constants[38] and a vacuum thickness of ~13 Å. For the $CeO_2(111)$, $H/CeO_2(111)$, $VO_n/CeO_2(111)$, and $VO_nH/CeO_2(111)$ structures, a (2×2) surface unit cell was employed with a $(3 \times 3 \times 1)$ k-mesh for the Brillouin zone integration. The atoms in the six top layers were allowed to relax, and those in the three bottom layers were fixed to their positions in the bulk.

The occupation of vanadium 3d or cerium 4f states is obtained by integrating the site- and angular momentum-projected spin-resolved density of states over spheres with radii chosen as the Wigner−Seitz radii of the PAW potentials.

3.2. Results. Whereas there is experimental evidence for the presence of monomeric vanadia species with vanadyl goups and vanadium in the +5 oxidation state, the number of oxygen atoms on vanadium is not known. To determine the structure of the thermodynamically stable monomeric species at a relevant oxygen partial pressure of 10^{-6} mbar, we have calculated surface-related free energies as a function of the temperature from the DFT+U energies.[35] Most stable in the 400−900 K range is the $VO_2/CeO_2(111)$ species, which is shown in Figure

(31) Shapovalov, V.; Metiu, H. *J. Phys. Chem. C* **2007**, *111* (38), 14179–14188.
(32) VASP.5.1.49, http://cms.mpi.univie.ac.at/vasp/.
(33) Beste, A.; Mullins, D. R.; Overbury, S. H.; Harrison, R. J. *Surf. Sci.* **2008**, *602*, 162–175.
(34) Ganduglia-Pirovano, M. V.; Sauer, J. *Phys. Rev. B* **2004**, *70*, 045422.
(35) Popa, C.; Ganduglia-Pirovano, M. V.; Sauer, J. Unpublished work.
(36) Fabris, S.; de Gironcoli, S.; Baroni, S.; Vicario, G.; Balducci, G. *Phys. Rev. B* **2005**, *72*, 237102.
(37) Castleton, C. W. M.; Kullgren, J.; Hermansson, K. *J. Chem. Phys.* **2007**, *127*, 244704.
(38) Da Silva, J. L. F.; Ganduglia-Pirovano, M. V.; Sauer, J.; Bayer, V.; Kresse, G. *Phys. Rev. B* **2007**, *75*, 045121.

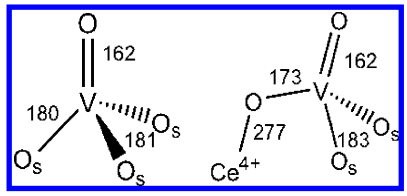

Figure 3. VO and VO_2 species on the defect-free $CeO_2(111)$ surface with bond distances in picometers.

2 (bottom middle). Figure 3 shows the coordination of the VO and VO_2 adspecies on the surface ions. The VO_2 adspecies has a terminal V=O group and with its second O atom it bridges to a Ce^{4+} surface ion. With its vanadium atom it attaches to two surface oxygen ions, resulting in a $O{=}V(O)_3$ unit with slightly distorted local C_s symmetry.

In contrast to a gas-phase VO_2 species in which the oxidation state of V is +4, that is, $V(d^1)$, in the $VO_2/CeO_2(111)$ system V is stabilized in the +5 oxidation state (d^0) by transferring one electron into Ce 4f states, creating a $Ce^{3+}(f^1)$ ion.

Hydrogen abstraction by a surface oxygen species has been identified as the rate-determining step in the ODH of propane and methanol.[13,14] In the case of methanol, the H atom is abstracted from a surface bound methoxy group:

$$O\}_{surf} + H\text{-}CH_2O\text{-}\}_{surf} \rightarrow HO\}_{surf} + {}^{\bullet}CH_2O\text{-}\}_{surf} \qquad (1)$$

One of the electrons of the dissociated C−H bond forms the $^{\bullet}CH_2O$- surface radical, whereas the other is transferred with the H atom to the surface oxygen site and results ultimately in a reduced metal ion. The Bronsted−Evans−Polyani (BEP) principle suggests a linear relationship between energy barriers and reaction energies for catalytic steps, such as reaction 1, which can be decomposed into C−H bond dissociation of the surface methoxy and hydrogenation of the surface oxygen species. When we consider different catalysts, the former is constant and, hence, the BEP suggests a linear relationship between the energy barriers and the hydrogenation energies of the surface oxygen species:

$$O\}_{surf} + \frac{1}{2}H \rightarrow HO\}_{surf} \qquad (2)$$

The energy of hydrogenation as reactivity descriptor has indeed been found to apply, for example, to the oxidative coupling of methane,[39] and its use has also been proposed[23] for selective C−H bond oxidation reactions in general.

Although reactivity parameters cannot replace the explicit calculation of energy barriers and rates (and do not always correlate with them; see, for example, ref 40 for methanol oxidation on MoO_3/TiO_2), they allow for a quick screening of several options and provide insights in crucial electronic factors. In the present study we calculate the hydrogenation energies

$$VO_n/CeO_2(111) + \frac{1}{2}H_2 \rightarrow VO_nH/CeO_2(111) \qquad (3)$$

and find that they explain the observed reactivity pattern. After the oxidation half-cycle has been completed, a water molecule is formed and an oxygen defect is created on the catalyst. Hence, the oxygen defect formation energy

$$VO_n/CeO_2(111) - \frac{1}{2}O_2 \rightarrow VO_{n-1}/CeO_2(111) \qquad (4)$$

is used as an additional descriptor for the activity of the oxidation catalyst.[24,41]

The more exoenergetic the hydrogenation energy is (and the lower the defect formation energy), the higher the activity of the catalyst is (and the lower the barrier). Hydrogen transfer (the rate-limiting step in oxidative dehydrogenation) leaves one electron on the catalyst, whereas oxygen defect formation (completing the oxidative dehydrogenation) leaves two electrons, which can occupy either V 3d or Ce 4f states. On the pristine $CeO_2(111)$ surface, the lowest oxygen defect formation energy (eq 4) has a value of 1.87 eV and is found for a subsurface oxygen site[42] (Figure 2, top left), which is consistent with recent experimental findings.[43] Creation of an oxygen defect in the $VO_2/CeO_2(111)$ structure requires 0.79 eV and yields the supported VO species shown in Figure 2 (bottom left). Hence, formation of an oxygen defect in the $VO_2/CeO_2(111)$ system requires ~1.1 eV less than for the uncovered CeO_2 support. The $O{=}V^{5+}(O_{surf})_3$ species formed (see Figure 3, left) consists of a terminal O=V group attached to three surface O ions on a nondefective $CeO_2(111)$ surface.[9] Moreover, V is also stabilized in the +5 oxidation state, that is, $V(d^0)$. The two electrons left in the system upon oxygen removal localize in 4f states on two (surface) Ce sites, reducing them to Ce^{3+}. This fits with the previously obtained result[44] that in $CeVO_4$ we do not have $V(d^1)^{4+}$ and $Ce(f^0)^{4+}$ but $V(d^0)^{5+}$ and $Ce(f^1)^{3+}$; that is, vanadium is in its highest oxidation state and cerium is reduced.

A completely analogous picture emerges from the calculated hydrogenation energies. For the $CeO_2(111)$ support, a hydrogenation energy of −1.21 eV is obtained (Figure 2, top right). Hydrogenation of the $VO_2/CeO_2(111)$ system yields a $VO_2H/CeO_2(111)$ structure (Figure 2, bottom left) with a reaction energy of −1.45 eV (eq 3); that is, hydrogenation is 0.24 eV more favorable than for the ceria support without vanadia being present. In the VO_2H structure, as in the oxygen-defective $VO_2/CeO_2(111)$ structure, V remains in the +5 oxidation state, whereas the ceria support is reduced. For an isolated vanadia species on silica, as considered in the study of the methanol oxidation mechanism,[13] the hydrogenation energy is +0.2 eV,[23] indicating much lower activity in ODH reactions than we find here for isolated vanadia on ceria (−1.45 eV). This explains the high-temperature formaldehyde desorption peak found for low loadings of vanadia on silica (675 K)[19] compared to the low-temperature peak at 370 K we report here (Figure 1).

The crucial point is that the reducibility of ceria does not diminish with the fraction of Ce^{3+} ions that are already present, because the additional electrons in Ce^{3+} occupy localized cerium f-states that do not interact with each other. As result, in contact with vanadia (or other redox-active oxides), ceria is always stabilizing their highest oxidation state.

We believe that the cooperativity revealed for the VO_x/CeO_2 system is special among the various vanadia supports, even among other redox-active supports such as TiO_2. VO_x/ZrO_2 and VO_x/TiO_2 are also known for increased methanol oxidation

(39) Sinev, M. Y.; Fattakhova, Z. T.; Lomonosov, V. I.; Gordienko, Y. A. *J. Nat. Gas Chem.* **2009**, *18* (3), 273–287.
(40) Kim, H. Y.; Lee, H. M.; Pala, R. G. S.; Metiu, H. *J. Phys. Chem. C* **2009**, *113*, 16083–16093.
(41) Kim, H. Y.; Lee, H. M.; Pala, R. G. S.; Shapovalov, V.; Metiu, H. *J. Phys. Chem. C* **2008**, *112*, 12398–12408.
(42) Ganduglia-Pirovano, M. V.; Da Silva, J. L. F.; Sauer, J. *Phys. Rev. Lett.* **2009**, *102*, 026101.
(43) Torbrügge, S.; Reichling, M.; Ishiyama, A.; Morita, S.; Custance, O. *Phys. Rev. Lett.* **2007**, *99*, 075433.
(44) Da Silva, J. L. F.; Ganduglia-Pirovano, M. V.; Sauer, J. *Phys. Rev. B* **2007**, *76*, 125117.

activity compared to VO_x/Al_2O_3 or VO_x/SiO_2,[2,5,6] but there are a variety of factors by which the support may affect the activity of the catalyst. DFT calculations have shown that the activity of supported (monolayer) vanadia clusters may increase with their size[23] and different supports (with different degree of hydroxylation) may lead to different size distributions. The different coordination of the vanadia clusters onto the surface of different oxides and different crystallographic surfaces of a given oxide play also a role. Some of these factors have been studied for the nonreducible ZrO_2 support in the $VO_x \cdot yH_2O/ZrO_2(101)$ and $VO_x \cdot yH_2O/ZrO_2(001)$ systems.[45] Computational studies[40,46] for the redox-active TiO_2 support have not yet led to a consistent answer why VO_x/TiO_2 is more active then VO_x/SiO_2.

Conclusions

From the present and a previous[9] combined experimental and computational study, we conclude that monomeric vanadia species on the ceria support are not reduced, but the support is. These species do *not* fully cover the support. Further reduction, specifically during the catalytic reaction, is particularly easy and results in an increase of the number of Ce^{3+} ions that have accepted one electron in their f-states. Both reactivity parameters, hydrogenation energy and O defect formation energy, indicate an enhanced activity of monomeric vanadia species on ceria surfaces as compared to the bare support but also compared to monomeric vanadia species on inert supports such as silica. This effect can also be considered as a promoting effect of the vanadia species on the activity of the uncovered ceria support. This effect explains the low-temperature α peak in the TPD spectra of adsorbed methanol in Figure 1, which is observed at coverages where primarily monomeric vanadia species have been identified. We conclude that the remarkably high activity observed for oxidation catalysts supported on ceria[2,6,7] as compared to other supports directly relates to this special synergy between the ceria support and the supported oxide.

Acknowledgment. This work has been supported by the Deutsche Forschungsgemeinschaft (Sonderforschungsbereich 546, Transition Metal Oxide Aggregates) and by a computer time grant of the Norddeutscher Verbund für Hoch- und Höchstleistungsrechnen (HLRN). H.A. and D.S. gratefully acknowledge financial support by the Alexander von Humboldt Foundation.

JA910574H

(45) Hofmann, A.; Ganduglia-Pirovano, M. V.; Sauer, J. *J. Phys. Chem. C* **2009**, *113*, 18191–18203.
(46) Goodrow, A.; Bell, A. T. *J. Phys. Chem. C* **2008**, *112* (34), 13204–13214.